Mechatronics 40 (2016) 41–50

Contents lists available at ScienceDirect

Mechatronics

journal homepage: www.elsevier.com/locate/mechatronics

An asymmetric cable-driven mechanism for force control of exoskeleton systems

Yeongtae Jung, Joonbum Bae*

Department of Mechanical Engineering, UNIST, Ulsan, Korea

ARTICLE INFO

Article history:
Received 28 May 2016
Revised 7 October 2016
Accepted 13 October 2016

Keywords:
Human-Robot interaction
Tendon/wire mechanisms
Force control

ABSTRACT

In this paper, an asymmetric cable-driven mechanism is proposed for accurate force control of exoskeleton systems with a compact structure. Inspired by the fact that the required forces in human motions are not symmetric in many cases, a spring-actuator type cable-drive mechanism is adopted, which enables a compact cable routing structure. The drive pulley is connected with the exoskeleton frame through a rotary series elastic mechanism to transmit the desired force to the human user. High performance in force control is achieved by advanced control algorithms, which combine a proportional and differential (PD) controller optimized by a linear quadratic (LQ) method with a disturbance observer (DOB) and a zero phase error tracking (ZPET) feedforward filter. The proposed system was tested for the elbow joint. Experimental results confirmed that the proposed system could generate and deliver accurate force to the human user even with external disturbances and modeling uncertainties introduced by human motions.

1. Introduction

Most of the weight of multi-degrees of freedom (DOFs) manipulators comes from directly mounted actuators. They become even heavier in case of series manipulators, because the proximal actuators are required to hold the weight of the distal actuators. To remove the heavy actuators and associated structures, cable-driven mechanisms have been adopted in many robotic manipulation systems [4,7,19,21,27,29,35,38]. In such cable-driven mechanisms, the actuators are placed at the base, and the force is transmitted through cables. Cable-driven mechanisms have also been widely applied in human-robot interaction systems, such as exoskeleton systems, because they enable a light and compact wearable structure [8,20,24] as shown in Fig. 1. Such exoskeleton systems were usually developed as rehabilitation and haptic devices for the communication with a virtual environment, which require precise force control. Also, their structures have to be compact to ensure safety of the users from collision, and to enhance the performance of system with less inertia.

However, the complex cable routing mechanisms and force control problems should be addressed to improve human-robot interactions with such a cable-driven mechanism. Because the cable-driven mechanism can transmit force with appropriate cable tension and routing, mechanical components, such as spring tensioners and idler pulleys, are typically used, which can make the cable-driven structure bulky and heavy. Also, flexible cables that can transmit only pulling forces provide challenges in delivering precise force to the human user. Bowden-cable mechanism, which is also called as a tendon-sheath actuation mechanism, have been researched because of its simple cable routing mechanism [5,12,14,31,33,36]. However, the friction between the tendon and sheath, backlash and hysteresis greatly lower the system performance. Since the disturbances mainly depend on the shape of sheath, it is hard to achieve precise force control in multi-DOF tendon-sheath actuation systems.

In this paper, a spring-actuator type cable-driven mechanism is proposed for force control of exoskeleton systems. In the proposed system, a linear spring acts as a power source as well as a tensioner by pulling the cable against the actuator. Because the required joint torques of human motions are not symmetric in many cases [1,23,28], the spring-actuator mechanism is a feasible solution with a simple cable routing structure and a self-tension mechanism. A rotary series elastic mechanism and robust control algorithms were applied with the cable-driven mechanism to enable high performance force control. Since the desired force can be delivered precisely with a simple cable routing structure, the proposed system is expected to be used in the exoskeleton systems for haptic and rehabilitation purpose that require precise force control and compact structures.

The remainder of this paper is organized as follows. The actuation mechanisms of previously developed cable-driven mechanisms and the proposed mechanism are described in Section 2.

* Corresponding author.
E-mail addresses: ytjung@unist.ac.kr (Y. Jung), jbbae@unist.ac.kr (J. Bae).

http://dx.doi.org/10.1016/j.mechatronics.2016.10.013
0957-4158/

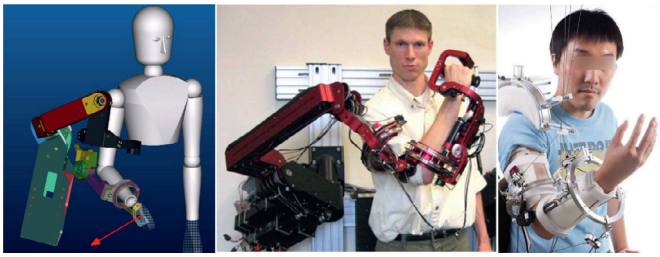

(a) L-EXOS [8] (b) CADEN-7 [24] (c) CAREX [20]

Fig. 1. Cable driven exoskeleton systems.

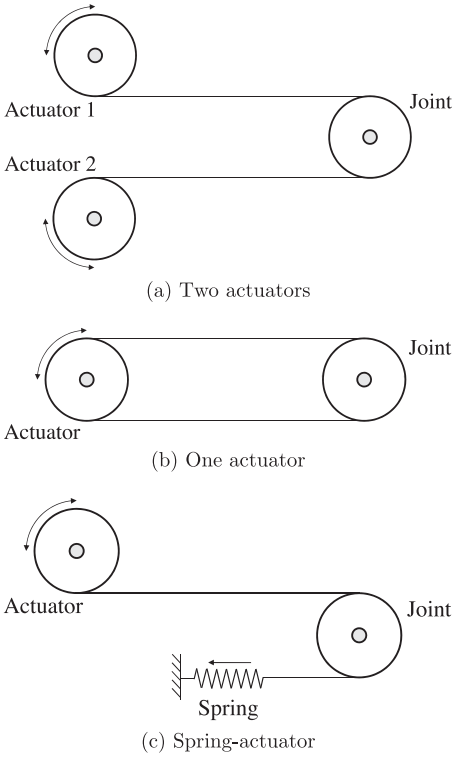

Fig. 2. Cable-driven mechanisms.

The dynamics and control structure of the proposed cable-driven mechanism is developed in Section 3, and the experimental results with the exoskeleton prototype for an elbow joint are shown in Section 4. Conclusions and future works are provided in Section 5.

2. Configuration of an asymmetric cable-driven mechanism

2.1. Cable-driven mechanism

In a cable-driven system, the torque generated by an actuator is transmitted though flexible cables. Because the cables can transmit forces only in the pulling direction, the cables pulled in two different directions are required for the actuation of one DOF rotational joint. To satisfy such requirements, the three structures in Fig. 2 have been used as basic cable-driven mechanisms.

In the first mechanism, two actuators pull each cable independently (Fig. 2a). This mechanism provides high performance and a relatively easy cable routing structure because the tensions of both cables are controlled by different actuators. Also, the joint stiffness can be adjusted easily by antagonistic control of the two actuators [19,34]. However, the number of required actuators is doubled compared with other mechanisms.

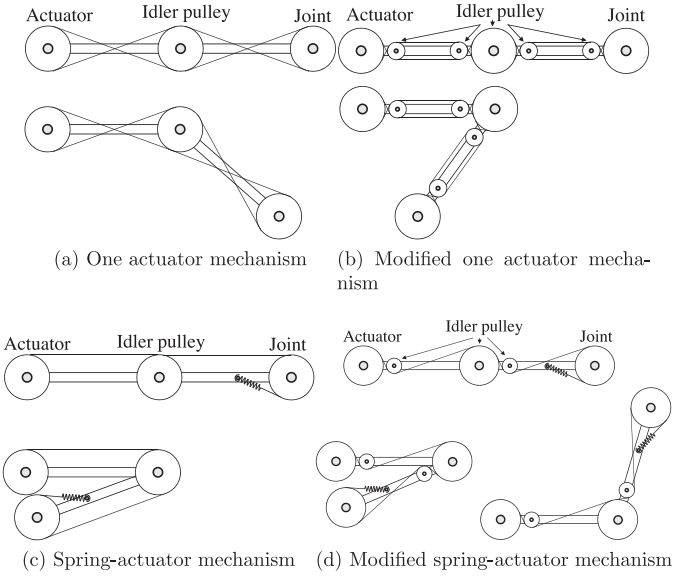

Fig. 3. Range of motions of the one actuator mechanism and the spring-actuator type mechanism.

In contrast, the mechanism shown in Fig. 2b can actuate one joint with one actuator. Due to its simple structure, it has been used for several robotic manipulators including exoskeleton systems [8,20,24,38]. Due to the nature of the mechanism, idler pulleys are required for routing the cables through other joints. However, one idler pulley cannot enlarge the range of motion sufficiently (Fig. 3a). The middle joint cannot be rotated further clockwise in this figure, because the lower routed cable will be separated from the idler pulley. Small additional idler pulleys can enlarge the motion range of joints (Fig. 3b), but this requires bulky structures in series manipulators with many DOFs. For example, a serial type 7-DOF exoskeleton may require six main idler pulleys and 12 small idler pulleys just at the first joint for the routed cable of the next six joints. Also, the cable of the non-pulled side is easily slackened, which causes backlash and slow responses. Thus, pretensioning mechanisms in the hardware and/or software are essential. For the pretension of cable-driven mechanisms, mechanical components, such as spring, idler pulleys and screws, were typically used [9,18,32,36]. Such tensioners made the cable-driven structure bulky and heavy, and required frequent adjustment for maintaining appropriate tension. Slack enable mechanisms were developed to use cable-driven systems in soft wearable robots without pretension in [3,13]. However, they are not applicable for pulley based cable-driven systems, because the slacked cable could be derailed from the pulley.

The spring-actuator mechanism, shown in Fig. 2c, uses an antagonistic spring for the actuation of one side, while the other side is driven by an actuator. The spring is pretensioned by pulling it with the actuator to apply two directional forces to the joint. The amount of force to the spring side is determined by this pretension and the stiffness of spring. The available actuator force is smaller than other mechanisms when the same actuator is used, because the actuator is required to pull the spring. However, as the spring naturally pulls the cable, the cable tension can always be maintained appropriately without additional components. More important thing is that its cable routing mechanism is much simpler than other mechanisms. The mechanism provides an almost full range of motion in the flexion direction without additional idler pulleys (Fig. 3c). When the joint requires extension motions, just one additional idler pulley for each proximal joint and itself is sufficient to enlarge the range of motion (Fig. 3d). Due to the sim-

Table 1
Elbow joint torque in flexion and extension [1].

	Flexion (kg· cm)	Extension (kg· cm)
Men	725 ± 154	421 ± 109
Woman	336 ± 80	210 ± 61

ple cable routing mechanism of the spring-actuator mechanism, it was adopted in some hand exoskeletons and robotic hands that requires compact structures [4,6,11,21,29,35].

2.2. Spring-actuator mechanism for asymmetric force requirement

The required joint torques of human motion are not symmetric in many cases, which inspired us to design an asymmetric actuating mechanism. One example of asymmetric joint torques is shown in Table 1. As shown in the table, the flexion torque of the human elbow joint is much larger than the extension torque, because the elbow joint is usually used to lift and carry objects against the gravity, which requires the flexional torque of elbow joint [1]. This asymmetry appears not only in the elbow, but also in the knee joint [23] and the finger [28] due to similar reasons.

Among the cable-driven mechanisms mentioned above, the first two mechanisms try to rotate the joint with the same force in both directions, but the spring-actuator mechanism can adjust the asymmetric force using a linear spring with an appropriate spring constant. As mentioned in the previous section, the motor is required to pull the linear spring at all time in the spring-actuator mechanism; thus, the available force is smaller than other cable-driven mechanisms. Therefore, the advantage, i.e. simple and light cable routing structures, may be shaded by the disadvantage. However, the asymmetry of the spring-actuator mechanism allows compensating the disadvantage by properly setting its asymmetry similar to the asymmetry of required torque.

Human joints are asymmetric in most cases, and the exoskeletons for human limbs usually require multiple DOFs in series, which leads to bulky and heavy cable routing structures. Thus, in this study, the spring-actuator mechanism, which allows a simple cable routing structure, was selected for the exoskeleton actuation mechanism.

2.3. Rotary series elastic mechanism

In human-robot interaction systems, force control is essential for intelligent interaction such as impedance control [10]. In this paper, a rotary series elastic mechanism is combined with a spring-actuator type cable-driven mechanism for force control. The series elastic mechanism has been widely used for human-robot interaction systems for force control and improved safety [2,16,25,26,33]. In the series elastic mechanism, an elastic element (i.e., a spring) is installed between the human and exoskeleton joint. By controlling the spring deflection, the force transmitted to the human can be controlled. In this research, a torsional spring is directly applied to the joint.

2.4. System configurations

A schematic of the proposed system is shown in Fig. 4. In this system, the drive pulley is rotated by a cable whose one end is connected with a motor and the other end is connected with a linear spring. As the motor rotates to the counterclockwise direction, the drive pulley is rotated in clockwise direction, and the linear spring is extended. In similar way, the linear spring pulls the drive pulley when the motor rotates to the clockwise direction. This drive pulley is connected with the exoskeleton frame via a torsional spring, which makes a rotary series elastic mechanism. By

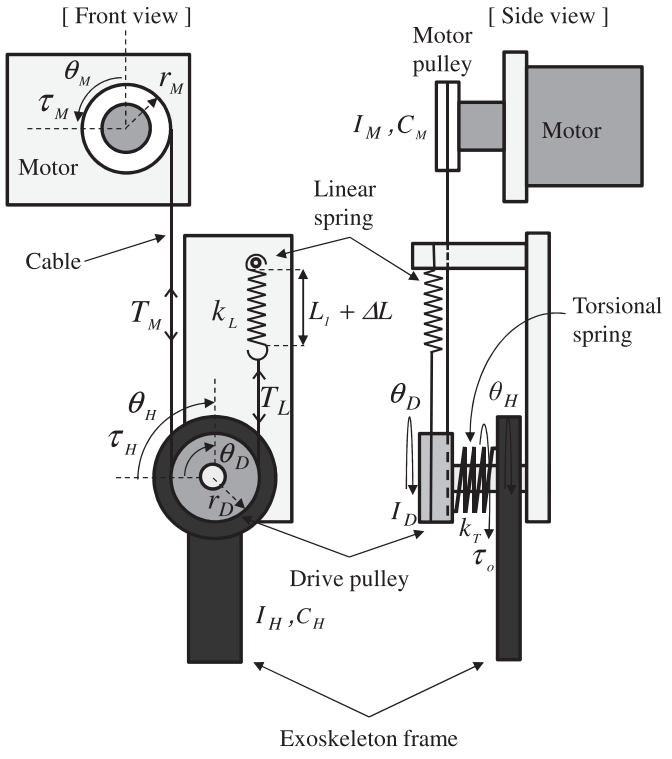

Fig. 4. Schematics of the proposed asymmetric cable-driven mechanism (Refer Section 3.1 for the notations in the figure.).

controlling the drive pulley angle to have an appropriate torsional spring deflection with respect to the exoskeleton frame worn by a human user, the series elastic mechanism enables to deliver the desired force accurately to the human user.

Because the linear spring is needed to prevent the cable slack and pull the cable, the spring is pretensioned as $L_1 - L_0$, where L_0 and L_1 are the free and pretensioned lengths of the linear spring, respectively. Thus, the linear spring generates the pulling force at least T_i as:

$$T_i = k_L(L_1 - L_0) \tag{1}$$

where k_L is the spring constant of the linear spring. Because the amount of pretension determines the force asymmetry, the pretension should be carefully designed considering required asymmetry force and structure stiffness.

3. Control of the asymmetric cable-driven system

3.1. System modeling

In the proposed system, the motor should be able to control the drive pulley position precisely so that the desired force can be transmitted to the human through the rotary series elastic mechanism. To find the relationship between the motor torque, τ_M, and the drive pulley angle, θ_D, the system in Fig. 4 is modeled as follows:

$$I_M\ddot{\theta}_M + C_M\dot{\theta}_M = \tau_M - T_M r_M \tag{2}$$

$$I_D\ddot{\theta}_D = r_D(T_M - T_L) + k_T(\theta_H - \theta_D) \tag{3}$$

$$I_H\ddot{\theta}_H + C_H\dot{\theta}_H = k_T(\theta_D - \theta_H) + \tau_H \tag{4}$$

where I_M and C_M are the inertia and damping coefficient of the motor, I_H and C_H are those of human, I_D is the inertia of the drive pulley, θ_M, θ_D and θ_H are the rotation angle of the motor, drive pulley and human, respectively, k_T is the spring constant of the torsional spring, r_M and r_D represent the pulley radius of the motor and drive pulley, respectively, T_M and T_L are the tension of each cable, τ_M is the motor torque and τ_H is the human torque.

By assuming that the appropriate cable tension is maintained by the linear spring, the relationship between the motor angle, θ_M, and the drive pulley angle, θ_D, is obtained kinematically as follows:

$$r_D\theta_D = r_M\theta_M \tag{5}$$

The linear spring is extended by ΔL from the pretensioned position, and the cable tension by the linear spring, T_L, is calculated by Hooke's law as follows:

$$\begin{aligned} T_L &= k_L(L_1 - L_0 + \Delta L) \\ &= k_L(L_1 - L_0 + r_D\theta_D) \end{aligned} \tag{6}$$

The output torque, τ_o, from the rotary series elastic mechanism is also calculated by deflection of the torsional spring as follows:

$$\tau_o = k_T(\theta_D - \theta_H) \tag{7}$$

By integrating (2)-(7), the drive pulley angle is expressed in the Laplace domain as follows:

$$\theta_D(s) = \frac{\frac{1}{r_M I'}}{s^2 + \frac{C'}{I'}s + \frac{k'+k_H}{I'}}(\tau_M(s) - \tau_i(s) + \tau'_H(s)) \tag{8}$$

where

$$I' = \frac{r_D}{r_M^2}I_M + \frac{1}{r_D}I_D \tag{9}$$

$$C' = \frac{r_D}{r_M^2}C_M \tag{10}$$

$$k' = k_L r_D \tag{11}$$

$$k_H(s) = \frac{1}{r_D}k_T(1 - k_T G_H) \tag{12}$$

$$G_H(s) = \frac{1}{I_H s^2 + C_H s + k_T} \tag{13}$$

$$\tau_i(s) = \frac{1}{s}r_M T_i \tag{14}$$

$$\tau'_H(s) = r_M G_H(s)\tau_H(s) \tag{15}$$

Note that G_H contains human-related parameters such as I_H and C_H, which are difficult to be measured. Even more, they are not constant values because physical properties of human muscle changes [37]. Thus, the nominal model of the system was obtained by letting I_H and C_H to zero for simplicity, and variation of such variables were dealt as modeling uncertainties. Then, G_H and k_H become to $\frac{1}{k_T}$ and 0, respectively. Thus, the nominal model of drive pulley angle is simplified as follows:

$$\theta_D(s) = \frac{\frac{1}{r_M I'}}{s^2 + \frac{C'}{I'}s + \frac{k'}{I'}}(\tau_M(s) - \tau_i(s) + \tau''_H(s)) \tag{16}$$

where $\tau''_H(s) = \frac{r_M}{k_T}\tau_H(s)$. The last term in (16) which is by human joint torque is treated as external disturbance to the controller. Both the modeling uncertainties and external disturbances caused by the interaction with human are compensated by robust control algorithms discussed in next section.

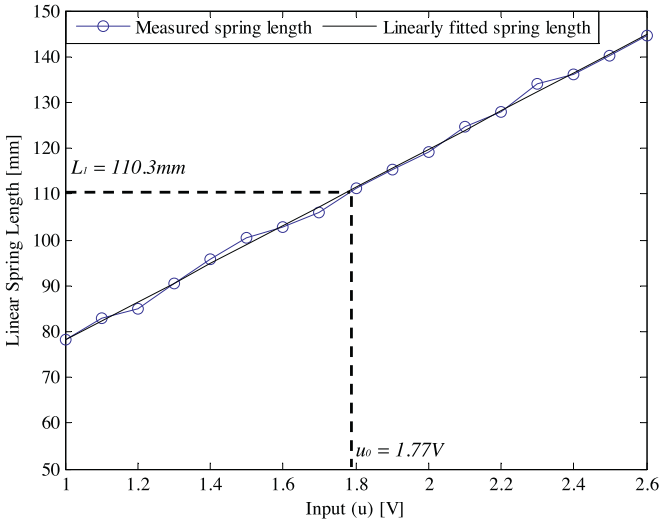

Fig. 5. Determination of u_0 by measured and linearly fitted linear spring length.

3.2. Controller design

A model-based robust control structure is proposed in this chapter for force control of the system. Because the system delivers the desired force to the human via the series elastic mechanism, the position control of drive pulley angle, θ_D, may be the main issue of the proposed control algorithms.

Before system identification, the initial linear spring force T_i was measured to compensate $\tau_i(s)$ from the system model in (8). As the motor input was increased gradually, the lengths of the linear spring in the stationary states were measured. In a stationary state, T_L and T_M can be assumed to be equal. Thus, the generated τ_M by the control inputs is the required torque to generate the same magnitude of T_M as T_L. Consequently, the input shows a linear relationship with the linear spring length as shown in Fig. 5. To calculate the input magnitude for compensating τ_i, the measured data were linearly fitted. The motor input to extend the linear spring to L_1 was calculated inversely from the fitted equation, and it is denoted by u_0 (i.e. u_0 generates T_M with the magnitude of T_i). In the system identification and the following experiments, the motor input, u, was set as :

$$u = u_c + u_0 \tag{17}$$

where u_c is the control input from the controller and u_0 is the input for compensating τ_i. Because u_0 generates motor torque with a magnitude of $r_M T_i$, the motor torque is expressed as :

$$\tau_M = \tau_c + \tau_i \tag{18}$$

Then, the system model in (8) is simplified to:

$$\theta_D(s) = \frac{\frac{1}{r_M I'}}{s^2 + \frac{C'}{I'}s + \frac{k'}{I'}}(\tau_c(s) + \tau''_H(s)) \tag{19}$$

The torsional spring was excluded during system identification because $\tau''_H(s)$ is treated as a disturbance in the position control. Thus, the system consisting of the motor, drive pulley, linear spring and cables was identified by sweeping sinusoidal signals, which have frequency from 1 Hz to 60 Hz with 2.5 V of magnitude. By fitting the parameters in (19) to the measured data as in Fig. 7, the nominal model of the system was identified as follows:

$$P_n(s) = \frac{15.41}{s^2 + 3.545s + 6.39} \tag{20}$$

As a basic controller, a proportional-differential (PD) controller was applied, whose gains were obtained by the linear quadratic

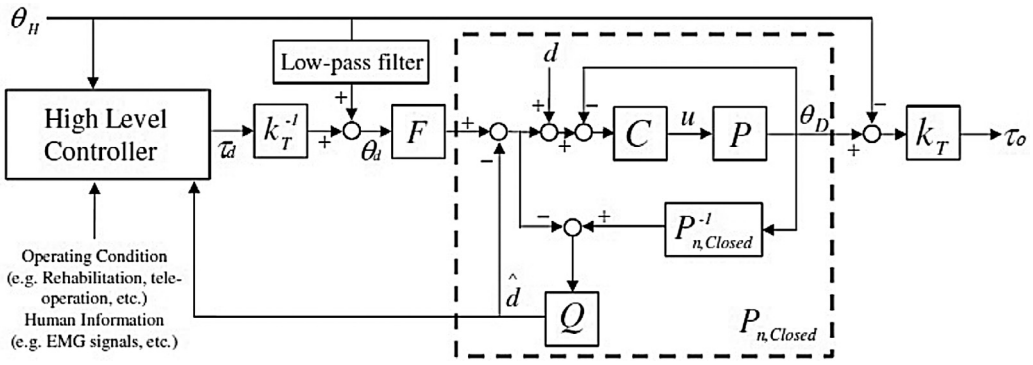

Fig. 6. Block diagram of the control structure. [θ_H is the position of exoskeleton in human side, d is a disturbance, τ_d is the desired torque determined by the high level controller, k_T is the torsional spring stiffness, F denotes the feedforward filter, C is the PD controller, P is the plant model of motor, $P^{-1}_{n,Closed}$ is the inverse of closed-loop transfer function of C and P, Q is the low-pass filter for the disturbance observer and τ_o denotes the output torque.].

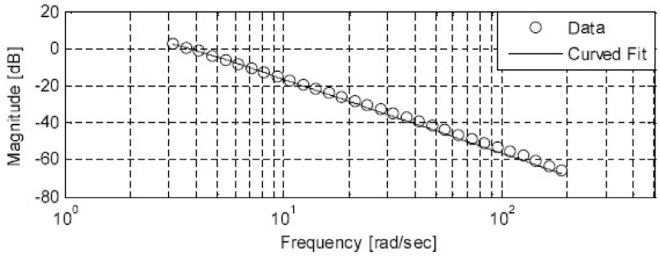

Fig. 7. Frequency response of the system.

(LQ) method. The LQ performance index is defined as follows:

$$J = \int_0^\infty (x^T Q x + u^T R u) dt \tag{21}$$

where x denotes the state, including the position and velocity of the motor, and u is the input. Q and R in (21) present the weighting factors of the position and speed of the drive pulley and of the control input, respectively. Using the performance index, the optimal PD gain was calculated for the controllable canonical form of (20).

The PD controller may not be sufficiently robust for this application, because an external disturbance and modeling uncertainties are introduced by interaction with human as in (19). Unlike the linear spring force, the disturbance introduced by human force and the modeling uncertainties cannot be directly compensated. Thus, a robust control algorithm is applied with the nominal model in (20). Disturbance observer (DOB) is one of the representative robust control algorithms, which can estimate and compensate the external disturbance [17]. The modeling uncertainties from a nominal model can be also compensated by dealing with the modeling uncertainties as equivalent disturbances. Thus, it is expected that the induced modeling uncertainties by in (19) can be canceled by the DOB.

To implement the DOB, we need to properly design the Q-filter to make the DOB algorithm realizable. Because the inverse of $P^{-1}_{n,Closed}(s)$ is not realizable, the Q-filter must have equal or higher relative order than that of $P_{n,\,Closed}$. Thus, $Q(s)$ was designed to have the same relative order of $P^{-1}_{n,Closed}(s)$ in this study. Because the maximum bandwidth of the human elbow is 4–6 Hz [22], the Q-filter was designed as a low-pass filter with a 10 Hz of cutoff frequency. The entire system was discretized with a sampling time of 1 ms for implementation in the digital control system.

Once the robustness of the closed-loop plant is secured by the DOB, a significant improvement in tracking performance can be expected by introducing a feedforward controller. In this study, the zero phase error tracking (ZPET) method was used [30]. Because

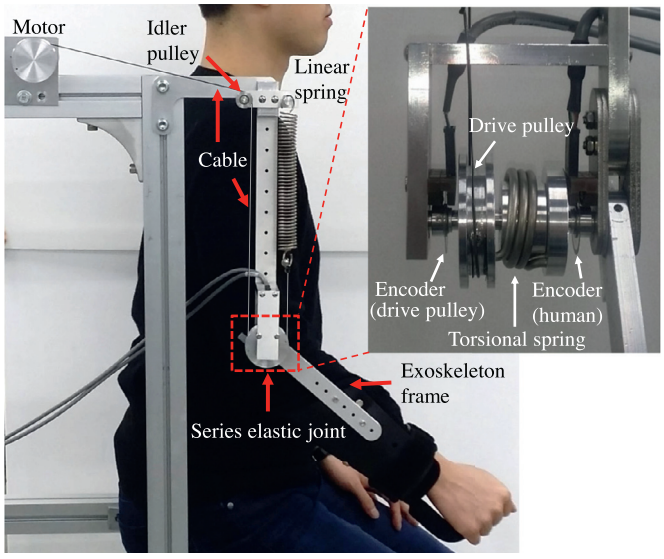

Fig. 8. A prototype of the proposed mechanism for the elbow joint.

the nominal model of the closed-loop is known, the ZPET controller, F, was designed as:

$$F = P^{-1}_{n,Closed} z^{-1} \tag{22}$$

The overall controller structure is shown in Fig. 6. Suppose the desired torque, τ_d, is given by a high level controller, which could be for rehabilitation or tele-operation, etc. Then, the desired drive pulley angle, θ_d, is calculated by the series elastic mechanism with the measured human joint angle, θ_H. By the DOB algorithm, the closed loop system is expected to act as $P_{n,\,Closed}$, and the ZPET controller, F, drastically improves the tracking performance. The measured drive pulley angle, θ_J, is used to make the output torque, τ_o with the measured human joint. A low-pass filter was applied to θ_H in determining θ_d, to reduce high frequency movement that may cause the instability of the DOB.

4. Experimental verification

4.1. Experimental setup

A one DOF upper limb exoskeleton with the proposed system was manufactured for the elbow as shown in Fig. 8. A linear spring, which generates a smaller force than the motor, was used for flexion motion, but it can also be positioned for extension motion for a different purpose. The specifications of equipment in the exper-

Table 2
Specifications of experimental setup.

	Specification
Motor	Maxon EC-4pole Gear ratio : 74:1 Nominal speed : 22.5 rad/s Nominal torque : 6.767 Nm
Driver	Maxon ESCON 70/10
DAQ	National Instruments PCIe-7841R
Encoder	US Digital, Incremental, 1250 CPR
CPU	Intel i7-3770
Operating System	Microsoft Windows 7
Software	National Instruments LabVIEW 2015

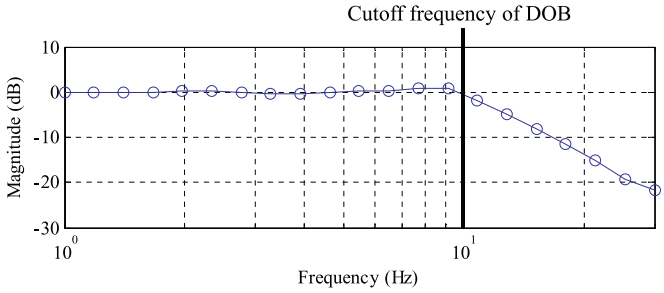

Fig. 9. Frequency response of the system without the torsional spring and human parts.

Table 3
Root mean square (RMS) errors in the experiments without a user.

Controller	Without disturbance (rad)	With disturbance (rad)
PD	0.0434	0.3587
PD+DOB	0.0419	0.0455
PD+DOB+ZPET	0.0045	0.0188

iment are shown in Table 2. The torsional spring was designed to have a spring constant of 1.17 Nm/rad, and the linear spring was designed to have a spring constant of 1.19 N/mm with initial length of 52.5 mm. The motor pulley and drive pulley had a radius of 21 mm. The pretension length was set to 110.3 mm considering the average required torque of the elbow joint in daily life, 1.4 Nm, could be generated at all times [24]. The maximum torque of the spring is 2.6 Nm at the maximum extension of the elbow. The expanded image in Fig. 8 shows the series elastic joint of the system. A torsional spring was placed between the drive pulley and the exoskeleton, and two encoders for the human joint and drive pulley were used to measure the spring deflection, thus torque transmitted to the human joint can be calculated.

4.2. Experimental verification without human interaction

The bandwidth of the closed loop system with proposed control algorithms was verified as shown in Fig. 9. The frequency response of the closed system was flat until about 10 Hz. Thus, the performance of the actuation part was sufficient to follow the motion of the elbow, which is up to 4∼ 6 Hz [22].

The position tracking performance of the system was tested with and without an intentional disturbance with three control methods: (a) PD controller, (b) PD controller and DOB, (c) PD controller, DOB and ZPET. In this experiment, the desired drive pulley angle was provided as pre-programmed arbitrary trajectory. The drive pulley was not connected to the torsional spring or human part. As shown in Fig. 10 and Table 3, the tracking errors of PD and PD plus DOB control were quite small; however, the tracking error of the PD, DOB plus ZPET control was extremely small compared with those of PD and PD plus DOB.

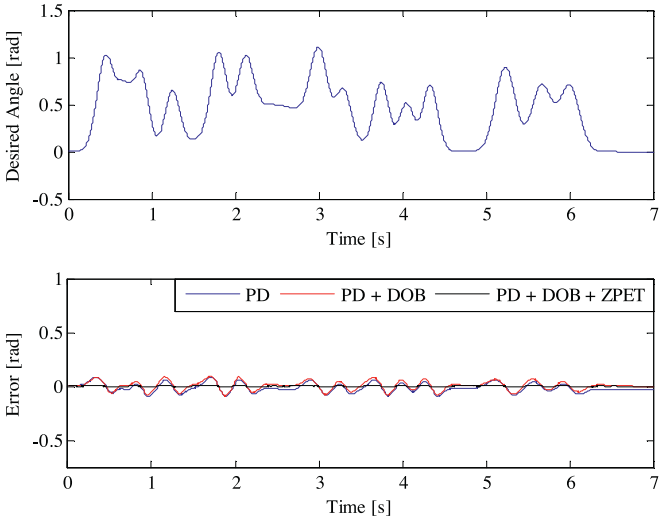

Fig. 10. Position tracking performance without inserting a disturbance. The torsional spring and human parts are excluded, i.e., no interaction with the user.

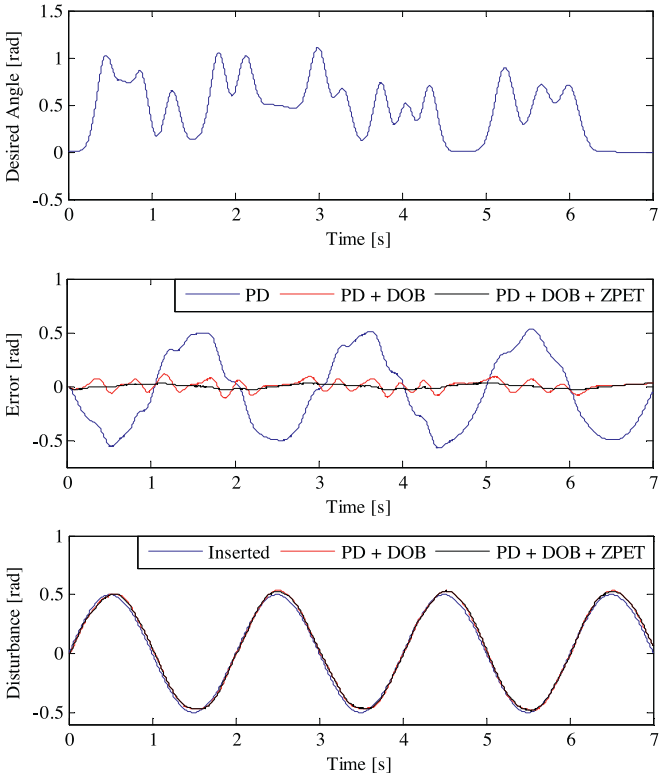

Fig. 11. Position tracking performance and the disturbance observation with a sinusoidal disturbance. The torsional spring and human parts are excluded, i.e., no interaction with the user.

However, the results changed significantly when an external disturbance was introduced. A sinusoidal disturbance was inserted in the digital controller as d in Fig. 6. Fig. 11 and Table 3 shows the experimental results with the same desired angle, with the intentional sinusoidal disturbance. In the PD controller case, the tracking error under PD control increased significantly. However, PD plus DOB controller maintained a similar level of tracking error as that without a disturbance. These results show that the DOB is capable of observing and rejecting the disturbance. The last graph in Fig. 11 compares the inserted disturbance and estimated disturbance by the DOB, confirming the performance of the DOB. Thanks

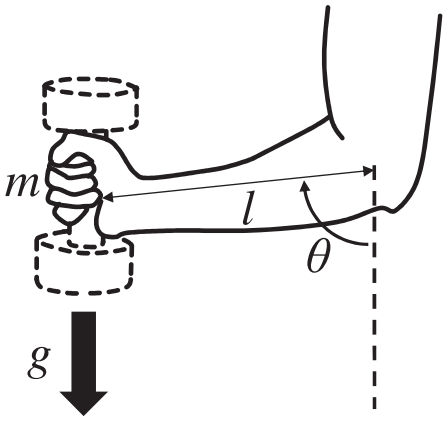

Fig. 12. Schematics and parameters for the virtual dumbbell experiment. m : mass of a virtual dumbbell, g : gravity, l : distance between the center of rotation of elbow joint and the hand, θ : elbow flexion angle.

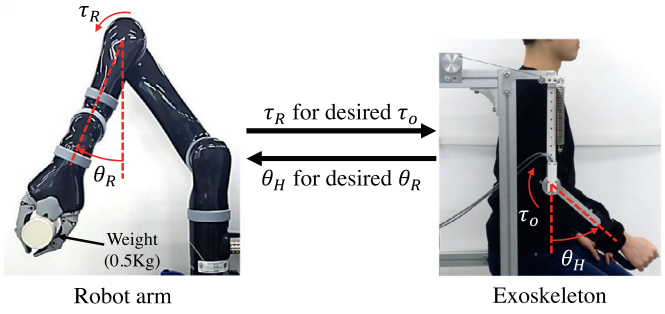

Fig. 13. Interaction between a robot arm and the exoskeleton. θ_R and θ_H are joint angles of the robot joint and the human elbow, τ_R is the measured reaction torque of the robot joint, and τ_o is the generated torque by the exoskeleton system.

to the robustness of the DOB, the use of the feedforward filter, ZPET, significantly increased the tracking performance similar to the previous experiment.

4.3. Experimental verification with human interaction

In the previous section, performance of the proposed mechanism without a human user was verified. However, its performance may depreciate if unknown disturbances are introduced by human interaction. To confirm that the system can transmit desired torque even with human interaction, the experiment with a human user was performed. As mentioned earlier, this mechanism is developed for the haptic interface with an exoskeleton structure; thus, the experiment with a human user is highly necessary.

In the experiments, the user wore the proposed exoskeleton system and moved arbitrarily. Four types of torques were applied to the system. First, the desired torque was set to zero to prove that this mechanism is enough back-drivable to ensure free motion of the user. The second type of torque was set as a sinusoidal torque, to verify that this mechanism can generate torque to both directions with given frequency. The third type of torque was set to the force from a virtual dumbbell as shown in Fig. 12, supposing the mechanism was applied in a haptic device for the communication with a virtual reality. Considering the inertia and gravity of the virtual dumbbell, the desired torque was set as follows, by assuming point mass.

$$\tau_d = ml^2\ddot{\theta} + mgl\sin\theta \tag{23}$$

The mass of the dumbbell, m, was set to 0.8kg, and the distance between the center of rotation of elbow joint and the hand, l, was

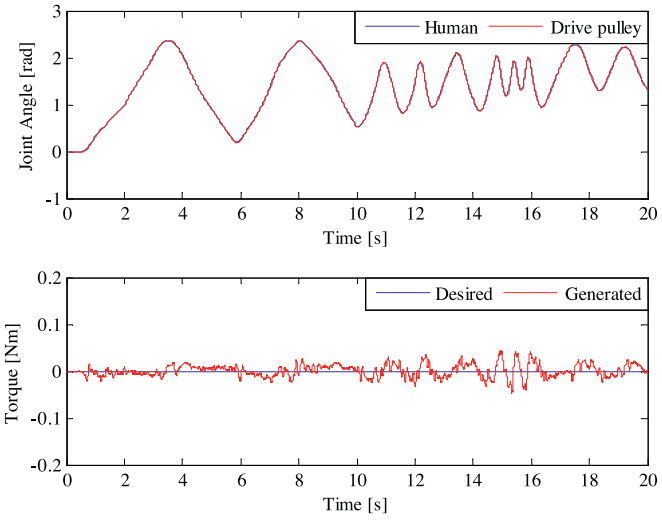

Fig. 14. Backdrivability test of the system.

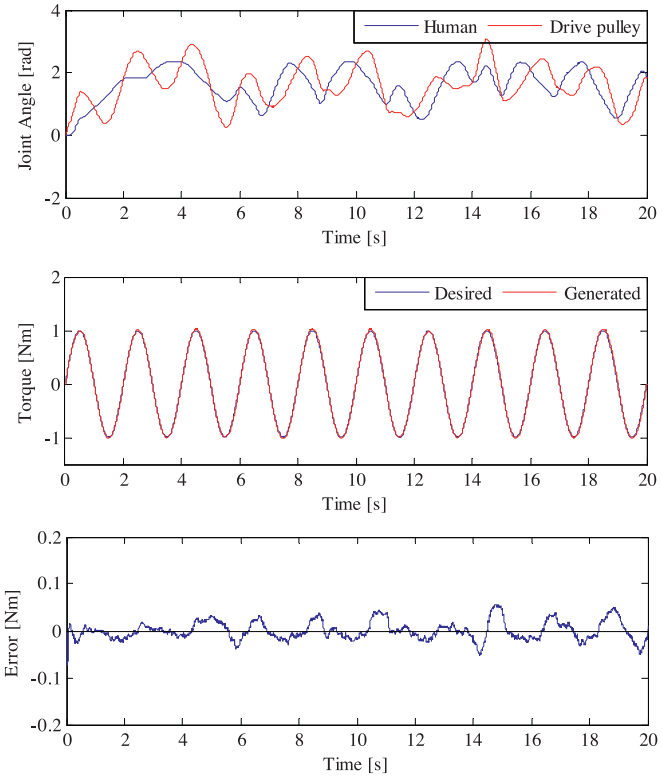

Fig. 15. Torque tracking performance with a human user and a sinusoidal desired torque.

set to 0.35m in the experiment. The range of elbow flexion angle, θ, was set to 0° to 135°.

In the last experiment, the desired torque was set to a measured torque of a robot arm, to test the feasibility as a haptic control interface with a robot arm. As shown in Fig. 13, a robot arm (Kinova, MICO [15]) was set to follow the motion of human elbow with holding a weight (0.5 Kg) using the measured elbow flexion angle from the exoskeleton. Meanwhile, the exoskeleton was set to generate the torque measured from the robot arm. The measured torque of the robot arm was scaled to 1/3 for this application. Because the robot arm and the exoskeleton were controlled by one computer, no time delay between them was occurred. In all experiments, the PD and DOB plus ZPET controllers were used to control the exoskeleton system.

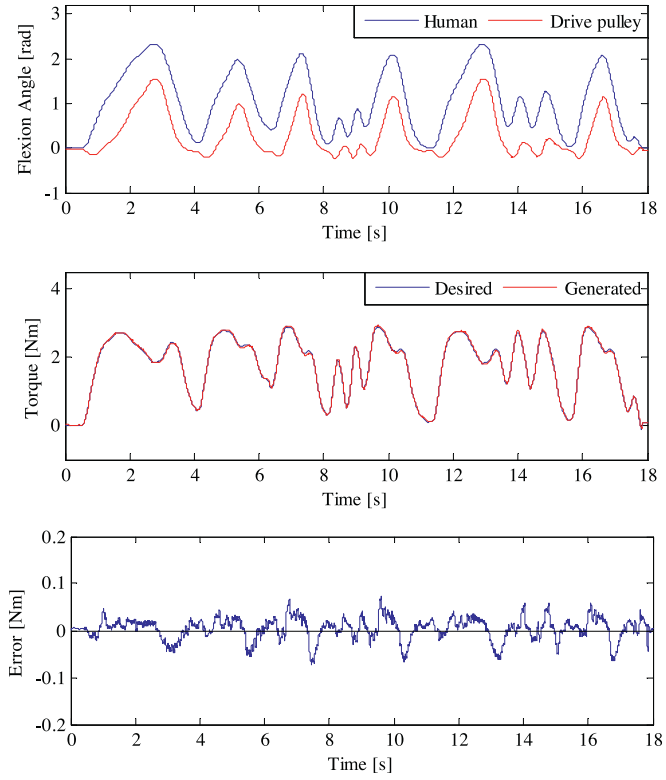

Fig. 16. Torque tracking performance of the system in the interaction with a virtual dumbbell.

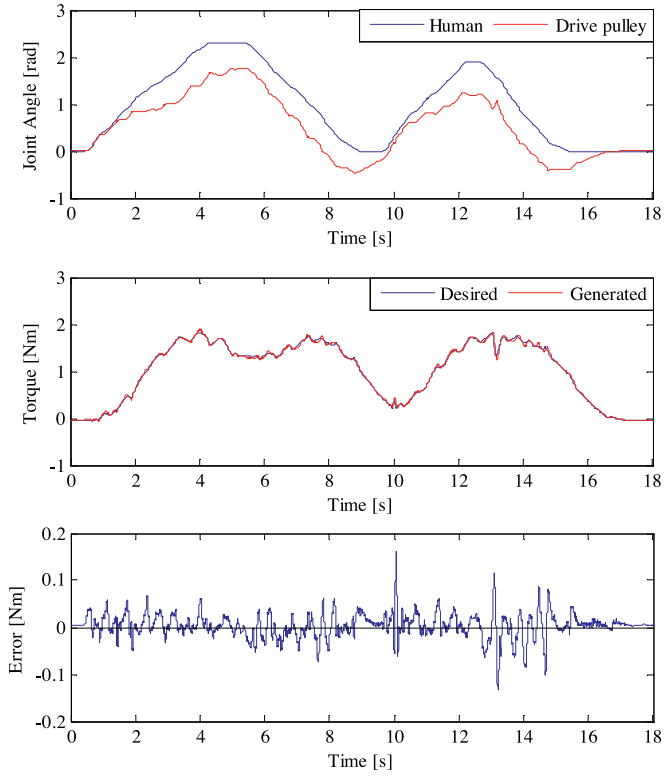

Fig. 17. Torque tracking performance in the interaction with a robot arm.

The experimental results are shown in Figs. 14, 15, 16 and 17 and summarized in Table 4. As shown in the experimental results, the system was back-drivable and could generate the desired torque accurately, even with the unpredictable and aperiodic human motion. The experimental results imply that the proposed mechanism and control strategy are suitable for force reflection to the joints that require asymmetric torque, and confirm that the user can feel the environment in the virtual space or around the robot through the proposed system.

Table 4
Root mean square (RMS) errors in the experiments with a user.

Experiment	RMS error (Nm)
Backdrivability	0.0133
Sinusoidal desired torque	0.0201
Interaction with a virtual dumbbell	0.0239
Interaction with a robot arm	0.0258

5. Conclusions

In this study, an asymmetric cable-driven mechanism for the force control of exoskeleton systems was developed. The mechanism had a linear spring in a cable for the joint, while the other cable was driven by the motor. A series elastic mechanism was used for the joint to enable force-mode control of the exoskeleton. A prototype of the exoskeleton for an elbow joint was manufactured to confirm the performance of the proposed mechanism. A proportional and differential (PD) controller with optimal gains for the nominal model of the position control system was used for control of the proposed system. Disturbance observer (DOB) and zero phase error tracking (ZPET) were applied in the control structure to compensate for the disturbances from the human and the system itself. The experimental results only with the actuator part confirmed the disturbance-rejection performance of the DOB and the tracking error reducing performance of the ZPET. The experimental results with the exoskeleton system showed that the proposed control algorithm had sufficient backdrivability and precise torque control performance, even in the interaction with a human user. The proposed mechanism is expected to be applied to multi-degrees of freedom (DOFs) exoskeleton systems for haptic or rehabilitation applications, which need compact structures and high performance in force control. In future work, exoskeletons with multi-DOFs, which will be used as a haptic control interface of the tele-operation of a robot arm, will be developed with the proposed mechanism.

Acknowledgement

This work was supported by the 2016 Research Fund (1.160005.01) of UNIST (Ulsan National Institute of Science and Technology), and Basic Science Research Program through the National Research Foundation of Korea (NRF) funded by the Ministry of Science, ICT & Future Planning (NRF-2015R1C1A1A01053763). A preliminary version of this paper was presented at the IEEE/RSJ International Conference on Intelligent Robots and Systems (IROS) 2016.

References

[1] Askew LJ, An K, Morrey BF, Chao EYS. Isometric elbow strength in normal individuals. Clin Orthop Relat Res 1987;222:261–6.
[2] Bae J, Kong K, Tomizuka M. Gait phase-based control for a rotary series elastic actuator assisting the knee joint. ASME J Med Devices 2011;5:031010.
[3] Cappello L, Binh DK, Yen S, Masia L. Design and preliminary characterization of a soft wearable exoskeleton for upper limb.. In: Proceedings of IEEE RAS/EMBS international conference on biomedical robotics and biomechatronics (BioRob); 2016. p. 623–30.
[4] Carrozza MC, Cappiello G, Micera S, Edin BB, Beccai L, Cipriani C. Design of a cybernetic hand for perception and action. Biol Cybern 2006;95:629–44.
[5] Cempini M, Cortese M, Vitiello N. A powered fingerthumb wearable hand exoskeleton with self-aligning joint axes. IEEE/ASME Trans Mechatron 2015;20:705–16.

[6] Chiri A, Vitiello N, Giovacchini F, Roccella S. Mechatronic design and characterization of the index finger module of a hand exoskeleton for post-stroke rehabilitation. IEEE/ASME Trans Mechatron 2012;17:884–94.
[7] Conti R, Meli E, Ridolf A. A novel kinematic architecture for portable hand exoskeletons. Mechatronics 2016;35:192–207.
[8] Frisoli A, Rocchi F, Marcheschi S, Dettori A, Salsedo F, Bergamasco M. A new force-feedback arm exoskeleton for haptic interaction in virtual environments. In: Symposium on haptic interfaces for virtual environment and teleoperator systems; 2005. p. 195–201.
[9] Grebenstein M, Chalon M, Fried W, Haddadin S, WimbÃ¶ck T, Hirzinger G, et al. The hand of the dlr hand arm system: designed for interaction. Int J Rob Res 2012;31:1531–55.
[10] Hogan N. Impedance control: an approach to manipulation: part i - theory, part II - implementation, part III - applications. J Dyn Syst Meas Control 1985;107:1–24.
[11] In H, Cho K. Jointless structure and under-actuation mechanism for compact hand exoskeleton. In: Proceedings of the IEEE international conference on rehabilitation robotics (ICORR); 2011. p. 1–6.
[12] In H, Kang BB, Sin M, Cho K. Exo-glove: a wearable robot for the hand with a soft tendon routing system view document. IEEE Robot Autom Mag 2015;22:97–105.
[13] Jeong U, In H, Lee H, Kang BB, Cho K. Investigation on the control strategy of soft wearable robotic hand with slack enabling tendon actuator. In: Proceedings of the IEEE international conference on robotics and automation (ICRA); 2015. p. 5004–9.
[14] Kaneko M, Wada M, Maekawa H, Tanie K. A new consideration on tendon-tension control system of robot hands. In: Proceedings of the IEEE international conference on robotics and automation (ICRA); 1991. p. 1028–33.
[15] Kinova. Mico. 2015. http://www.kinovarobotics.com/.
[16] Kong K, Bae J, Tomizuka M. Control of rotary series elastic actuator for ideal force-mode actuation in human-robot interaction applications. IEEE/ASME Trans Mechatron 2009;14:105–18.
[17] Lee H, Tomizuka M. Robust motion controller design for high-accuracy positioning systems. IEEE Trans Ind Electron 1996;43:48–55.
[18] Lens T, Kunz J, von Stryk O. Biorob-arm: a quickly deployable and intrinsically safe, light-weight robot arm for service robotics applications.. In: International Symposium on Robotics (ISR); 2010. p. 905–10.
[19] Ma S, Hirose S, Yoshinada H. Design and experiments for a coupled tendon–driven manipulator. Control Syst IEEE 1993;13:30–6.
[20] Mao Y, Jin X, Dutta GG, Scholz JP, Agrawal SK. Human movement training with a cable driven arm exoskeleton (carex). IEEE Trans Neural Syst Rehabil Eng 2015;23:84–92.
[21] Massa B, Roccella S, Carrozza MC, Dario P. Design and developement of and underactuated prosthetic hand. In: Proceedings of the IEEE International Conference on Robotics and Automation (ICRA); 2002. p. 3374–9.
[22] Neilson PD. Speed of response or bandwidth of voluntary system controlling elbow position in intact man. Med Biol Eng 1972;10:450–9.
[23] Neilson PD. Biomechanical analysis of knee flexion and extension. J Biomech 1973;6:79–92.
[24] Perry JC, Rosen J, Burns S. Upper-limb powered exoskeleton design. IEEE/ASME Trans Mechatron 2007;12:408–17.
[25] Pratt JE, Krupp BT, Morse CJ, Collins SH. The roboknee: an exoskeleton for enhancing strength and endurance during walking. In: Proceedings of the IEEE international conference on robotics and automation (ICRA); 2004. p. 2430–5.
[26] Ragonesi D, Agrawal S, Sample W, Rahman T. Series elastic actuator control of a powered exoskeleton. In: Annual international conference of the IEEE EMBS; 2011. p. 3515–18.
[27] Rifa H, Mohammed S, Hassani W, Amirat Y. Nested saturation based control of an actuated knee joint orthosis. Mechatronics 2013;23:1141–9.
[28] Sofia B, Anna N, Eja P, Ann B, Carina T. Relationship between finger flexion and extension force in healthy women and women with rheumatoid arthritis. J Rehabil Med 2012;44:605–8.
[29] Srl P. IH2 Azzurra; 2015. http://www.prensilia.com/
[30] Tomizuka M. Zero phase error tracking algorithm for digital control. J Dyn Syst Meas Control 1987;109:349–54.
[31] Tsuji K, Soeda Y, Nagatomi H, Kitajima M, Morikawa Y, Ozawa S, et al. Free allocation of actuator against end-effector by using flexible actuator. In: Proceedings of the IEEE international workshop on advanced motion control (AMC); 2006. p. 329–33.
[32] Vanderborght B, Tsagarakis NG, Ham RB, Thorson I, Caldwell DG. Maccepa 2.0: compliant actuator used for energy efficient hopping robot chobino1d. Autonom. Robot. 2011;31:55–65.
[33] Veneman JF, Kruidhof R, Hekman EE, Ekkelenkamp R, Asseldonk EHV, van der Kooij H. Design and evaluation of the lopes exoskeleton robot for interactive gait rehabilitation. IEEE Trans. Neural Syst. Rehab. Eng. 2007;15:379–86.
[34] Viteiello N, lenzi T, Rossi SMD, Roccella S, Carrozza MC. A sensorless torque control for antagonistic driven compliant joints. Mechatronics 2010;20:355–67.
[35] Walkler R. Developments in dextrous hands for advanced robotic applications. In: Proceedings of the sixth biannual world automation congress; 2004. p. 123–8.
[36] Wu Q, Wang X, Chen L, Du F. Transmission model and compensation control of double-tendon-sheath actuation system. IEEE Trans Ind Electron 2015;62:1599–609.
[37] Zajac FE. Muscle and tendon: properties, models, scaling, and application to biomechanics and motor control. Crit Rev Biomed Eng 1989;17:359–411.
[38] Zinn M, Roth B, Khatib O, Salisbury JK. A new actuation approach for human friendly robot design. Int J Rob Res 2004;23:379–98.

Yeongtae Jung received the B.S. degree in mechanical and advanced materials engineering from the Ulsan National Institute of Science and Technology (UNIST), Ulsan, Korea, in 2013. Since 2013, he has been working toward the Ph.D. degree in mechanical engineering at UNIST. His current research interests include wearable robotics, rehabilitation robotics, and human-machine interface. Mr. Jung received the Global Ph.D. Fellowship in 2013.

Joonbum Bae received the B.S. degree (summa cum laude) in mechanical and aerospace engineering from Seoul National University, Seoul, Korea, in 2006, and the M.S. and Ph.D. degrees in mechanical engineering from the University of California at Berkeley, Berkeley, CA, USA, in 2008 and 2011, respectively, where he also received the M.A. degree in statistics in 2010. In 2012, he joined the School of Mechanical and Nuclear Engineering, Ulsan National Institute of Science and Technology (UNIST), Ulsan, Korea, where he is currently the Director of the Bio-Robotics and Control Laboratory. His current research interests include modeling, design, and control of human-robot interaction systems for virtual reality, teleoperation, and rehabilitation, and biologically inspired robot systems. Dr. Bae was a finalist of the Semi-plenary Paper Award at the ASME Dynamic Systems and Control Conference in 2012, and a finalist of the Best Poster Paper Award at the IFAC World Congress in 2008. He received a Samsung scholarship during his Ph.D. studies.